

## A CASE STUDY IN BACKLASH CHARACTERIZATION IN MECHANICAL SYSTEMS

T. Tjahjowidodo, F. Al-Bender, H. Van Brussel  
*Mechanical Engineering Department*  
*Division PMA, Katholieke Universiteit Leuven*  
*Celestijnenlaan 300B, B3001 Heverlee, BELGIUM*  
*tegoeh.tjahjowidodo@mech.kuleuven.ac.be*

### ABSTRACT

The Frequency Response Function (FRF) method using an experimental analysis such as free vibration with shock excitation or forced vibration with step or chirp excitation has proven to be a most efficient way to identify the modal parameters of mechanical structures. However, there is a limitation that only linear dynamic systems can be tested through these methods. The problem becomes more complex when nonlinear systems have to be identified. If the nonlinear system is 'well-behaved', i.e. if it shows periodic response to a periodic excitation, 'skeleton' identification techniques may be used to estimate the modal parameters, in function of the amplitude and frequency of excitation. However, under certain excitation conditions, chaotic behaviour might occur so that the response is aperiodic. In that case, chaos quantification techniques, such as Lyapunov exponent, are proposed in the literature. This paper deals with the application of the aforementioned nonlinear identification techniques to an experimental mechanical system with backlash. It compares and contrasts Hilbert transforms with Wavelet analysis in case of skeleton identification showing their possibilities and limitations. Chaotic response, which appears under certain excitation conditions and could be used as backlash signature, is dealt with both by a simulation study and by experimental signal analysis after application of appropriate filtration techniques.

### INTRODUCTION

Frequency Response Function (FRF) method utilizing a free vibration response after a shock excitation (or forced vibration response using a variety of excitation signals) is found to be a very practical way for modal parameters estimation of many mechanical systems. This method is however limited only to linear systems. The problem becomes more complex when nonlinear systems have to be identified. In

order to overcome this difficulty, some researchers often characterize nonlinear systems using Volterra and Wiener series [1], while other techniques taken as an extension of linear theory ARMA, namely NARMA and NARMAX have also been developed and proposed for different systems for the purpose of identification [1,2]. Another simple but elegant way to characterize the system is by utilizing the Hilbert transform technique [3].

The Hilbert transform is an integral transform of the same family as the Fourier transform. The difference is in the kernel function and instead of transforming a time-domain function to its frequency-domain, it transforms the signal to the imaginary part of the analytical function. By definition [4]: Hilbert transform is a mathematical transform that shifts each frequency component of the instantaneous spectrum by  $p/2$  without affecting the magnitude. Tomlinson [5] shows that the Hilbert transform is an effective mathematical tool, which allows one to investigate the causality, stability and linearity of systems. The Hilbert transform of the FRF of a linear structure reproduces the original FRF, and any departure from this can be attributed to non-linear effects. Feldman [6] has proposed methods of *FreeVib*, which identifies the modal parameters of the system by free vibration analysis. The analysis of the transient response of the system, which is obtained after short duration of excitation, commonly appears for linear system identification, since it contains direct information of the damping (from the decay of the response) and the stiffness characteristic (from the frequency content of the response). However, this technique is not immediately applicable for nonlinear system identification where the natural frequencies are amplitude dependent. The function relating the natural frequencies to the amplitude, namely the so-called skeleton curve, of a nonlinear system shows a deviation from the horizontal straight line of the linear system case. Every typical geometric nonlinearity in mechanical structures, which manifests itself as a change in the modal parameters of a

structure with changes in the structure deformations during motion, has a unique form of the skeleton curve. The analysis of the topography of the skeleton curve for different nonlinear modal parameters is summarized in reference [7]. Therefore, extraction of the instantaneous properties plays an important role in the completion of the skeleton curve as the result, and Hilbert transform offers one of the most successful approach to extracting the envelope and instantaneous frequency. If we make the complex sum of the original signal with the Hilbert transform of it in imaginary form, we will obtain the complex form of the original signal, namely the analytic signal. The modulus of this signal will give us the instantaneous amplitude, whilst the derivative of its argument represents the instantaneous frequency of the original signal. Extensive studies on the effectiveness of extracting the instantaneous amplitude and frequency can be found in [8,9], while Davies and Hammond [10] compared and contrasted the application of Hilbert transform with another analysis technique known as ‘method of slowly varying amplitude and phase’ for this extraction purpose. Practical application of this technique for damage diagnosis purpose of rotors was presented by Feldman and Seibold [11]. While Wang et al. [12] proposed a relatively new approach similar to the skeleton curve, namely the skeleton linear model (SLM). They related the (slowly time-varying) modal parameters of a system by using quadratic time-frequency distribution of its instantaneous response. This indicates the skeleton curve in an almost distinct way. Based on the obtained skeleton curve, after some mathematical manipulations, the estimated characteristics of the restoring and damping forces can be provided.

However, for a great number of real engineering systems, in particular those with high damping, free vibration analysis is not possible due to the fact that the transient response occurs in a very short time duration so that the observation sample is not adequate for *FreeVib* identification. In order to overcome this problem, Feldman proposed the *ForceVib* method [13]. In this method, the system under investigation is excited using a suitable excitation input and after some mathematical manipulation, the skeleton curve can be obtained as a function of the envelope and the instantaneous frequencies of the output response as well as the excitation input.

Despite of its effectiveness and simplicity, Hilbert transform based of instantaneous properties extraction has some limitations. Extraction of the envelope signal and its instantaneous frequency using Hilbert transform is strictly exact only if the real-value signal is asymptotic, where the signal has slowly varying amplitudes compared with the phase variations. In particular Ruzzene et al. [14] demonstrate that this technique introduces more errors when high damping is present in the system. Even if asymptotic signals are used, the Hilbert transform method requires a signal filtration. In order to resolve this problem, Feldman and Braun [15] offered the use of the Wigner-Ville Distribution to complement the Hilbert transform analysis in refining the extraction results. Nevertheless, this concept does not offer direct extraction result

of the instantaneous properties of the signal under observation. Moreover, the instantaneous amplitude of the corresponding signal cannot be estimated very well. This can be understood, since the Wigner-Ville Distribution does not offer an accurate modulus of time-frequency components.

Meanwhile, the Wavelet transform technique has gained popularity in the area of time-frequency representation (TFR) study and system identification field. This technique is actually developed as an alternative approach to the Short Time Fourier Transform to overcome the resolution problem in the latter transformation technique. Compared to Wigner-Ville Distribution, as another alternative to TFR, the Wavelet transform has more accurate modulus time-frequency component. Ghanem and Romeo [16] presented an identification technique of linear time-varying dynamical system contaminated with noise using the Wavelet transform, while Lenaerts et al. [17] validated the Wavelet transform and the Restoring Force Surface method for identification purpose using an experimental testbed. Staszewski [18] extensively demonstrated the application of identification of geometrical nonlinearity in the mechanical structures. He extracted the instantaneous properties of the transient response using the ridges of its Wavelet transform and reconstructed the skeleton curve to identify the modal parameters in the system. He also extended his analysis to the identification of a two-degree-of-freedom system. In a subsequent paper, Staszewski and Chance [19] verified the corresponding theoretical study on a real experimental setup. They implemented the identification technique on a test rig comprising a mass suspended on a nonlinear spring. The test setup was designed and built in such a way as to minimize the damping in the system. Therefore, the transient response of the system after shock excitation can be observed sufficiently. However, there are hardly any instances in the literature of the application of those types of system identification to systems comprising high damping.

Up to this point, we have assumed that the system is ‘well-behaved’ in the sense that its response is periodic for a periodic excitation. However, under certain conditions in dynamical systems (specifically nonlinear mechanical systems) chaotic behavior might occur, rendering the above mentioned techniques inapplicable. Lin [20] found that a simple mass-spring-damper system comprising backlash element might give chaotic response under certain excitation condition. He also demonstrated this behaviour in a supported beam with a mass at its midpoint. A backlash stiffness nonlinearity was introduced by providing motion constraints on both sides of the mass. However, he did not present the chaos quantifiers and correlate the quantification to the model parameters of his system. Theodossiades et al. [21] showed the chaotic responses in a more complex system, namely a gear pair system with backlash and periodic stiffness, under different condition. Feng et al. [22] studied the chaotic response on a model of a rattling system and presented the bifurcation diagram of the chaotic behaviour as a function of excitation frequency and amplitude. Trendafilova et al. [23] tried to exploit the chaos quantifiers for

fault detection in a real robot joint. They used the high-frequency component of the response besides the excitation frequency to quantify the chaoticity, and correlate it with the backlash size in the robot joint. However, the route of chaos in this high-frequency component signal was not exploited.

In the first place, this paper presents such a practical application to a single degree of freedom mechanical system with a backlash component by observing a forced response of the system under certain excitation, when the free vibration response is almost impossible to be observed. Subsequently, this paper attempts to correlate the chaos quantifiers (e.g. Lyapunov exponent ( $\lambda$ ) and Correlation Dimension), with the modal parameters of a chaotic system, in particular, for our case, the backlash size. Such correlation methodology could be further developed so as to deal with other nonlinear systems such as defect qualification and quantification. Early damage detection in a mechanical system is another possibility to exploit the model. At the end, this paper confirms experimentally the possible presence of chaotic response in a real mechanical system and characterises it.

In the following, section 1 describes the theoretical basis of the methods including some simulations. Section 2 describes the experimental setup, formulates a detailed mechanical model of the system, analyzes the obtained data and discusses the results, respectively. Finally, appropriate conclusions are drawn in Section 3.

## NOMENCLATURE

- $A(t)$  : amplitude envelope of a signal  
 $y(t)$  : instantaneous phase of a certain signal  
 $\tilde{x}(t)$  : Hilbert transformed of a certain signal  $x(t)$   
 $x_0$  : backlash degree  
 $\alpha$  : dimensionless form of backlash, which is inversely proportional to  $x_0$  and linearly proportional to amplitude of excitation  
 $\lambda$  : Lyapunov exponent

## 1 THEORETICAL BASIS AND SIMULATION

### 1.1 Skeleton Identification

The skeleton technique enables us to identify the ‘instantaneous’ modal parameters, including restoring force and damping force, for a certain class of nonlinear systems, through analysing their free or forced response by methods such as the ones described in the following.

#### 1.1.1 Hilbert Transform

A large number of signals, including vibration of nonlinear system can be converted to an analytic signal in complex-time and represented in the form of the combination of envelope and instantaneous phase [3,7]:

$$Y(t) = y(t) + j\tilde{y}(t) = A(t) \cdot e^{j\varphi(t)} \quad (1)$$

where  $\tilde{y}(t)$  is the Hilbert Transform of the real-valued signal  $y(t)$ ,  $Y(t)$  is an analytic signal in complex-time function,  $A(t)$

and  $\varphi(t)$  are an envelope (amplitude) signal and an instantaneous phase respectively.

We now consider that the forced vibration equation of a single-degree-of-freedom system could be written as:

$$\ddot{y} + 2h_0(A)\dot{y} + \omega_0^2(A)y = F/m \quad (2)$$

where  $y$  is the response signal,  $F$  is the forced excitation signal,  $m$  is the mass of the system,  $h_0$  and  $\omega_0$  are symmetrical viscous damping and stiffness characteristic of the system, respectively, which depend on the amplitude,  $A$ . According to the main properties of non-overlapping spectra of Hilbert Transform, Feldman [13] shows that equation (2) can be converted by Hilbert Transform to the complex form:

$$\dot{Y} + 2h_0(A)\dot{Y} + \omega_0^2(A)Y = F/m \quad (3)$$

where  $Y(t) = A(t) \cdot e^{j\varphi(t)}$  is an analytic signal of a solution of the system and  $F(t)$  is the analytic signal of the forced excitation in complex-time form.

Substituting the analytic signal forms of  $Y(t)$  and  $F(t)$  together with the two derivatives of  $Y(t)$  in equation (3), the representation of the corresponding modal parameters can be derived:

$$\omega_0^2(t) = \omega^2 + \frac{\alpha(t)}{m} - \frac{\beta(t)\dot{A}}{A\omega m} - \frac{\ddot{A}}{A} + \frac{2\dot{A}^2}{A^2} + \frac{\dot{A}\dot{\omega}}{A\omega} \quad (4a)$$

$$h_0(t) = \frac{\beta(t)}{2\omega m} - \frac{\dot{A}}{A} - \frac{\dot{\omega}}{2\omega} \quad (4b)$$

where  $\omega$  is time derivative of the instantaneous phase  $\varphi$ , while  $\alpha$  and  $\beta$  are the real and imaginary parts of the ratio  $\frac{F(t)}{Y(t)} = \alpha(t) + j\beta(t)$ , respectively.

#### 1.1.2 Wavelet Transform

Wavelet analysis is done in a similar way to the Short Time Fourier Transform (STFT), in the sense that the signal is multiplied by a function (i.e. *mother wavelet*, similar to the window function in STFT), and the transform is computed separately for different segments of the time-domain signal. The main difference between Wavelet Transform and STFT is the width of the ‘window’ in Wavelet Transform, which changes as the transform is computed for every single spectral component. Therefore, Wavelet analysis allows the use of long time intervals where we want more precise low-frequency information, and shorter regions where we want high-frequency information. The Wavelet Transform of real-value signal  $y(t)$  is defined as follows:

$$W(s, \tau) = \frac{1}{\sqrt{|s|}} \int_{-\infty}^{+\infty} y(t) \psi^* \left( \frac{t - \tau}{s} \right) dt$$

As seen in the equation above, the transformed signal is a function of **translation**,  $\tau$ , which corresponds directly to time, **scale/dilation** ( $s$ ), which relates to frequency information indirectly, and  $\psi(t)$  as a **mother wavelet**. Different researchers have proposed several families of mother wavelet functions.

The mother wavelet function, which will be used in this paper, is the popular function of Complex Morlet Wavelet [24]:

$$\Psi(t) = \sqrt{\pi f_b} \cdot e^{j\omega_c t} \cdot e^{-t^2/f_b} \quad (5)$$

where  $f_b$  is the bandwidth parameter and  $\omega_c = 2\pi f_c$  is the centre frequency.

### Envelope and Instantaneous Frequency Extraction

Energy density distribution over the  $(s, \tau)$  scale-translation plane can be represented by the square of the modulus of Wavelet transform. The energy of a signal is mainly concentrated on that plane around the so-called ridge of the wavelet transform. This ridge is directly related to the instantaneous frequency of the signal. Tchamitchian et al. [25] formulated the relation of the instantaneous frequency and the ridge as follows:

$$s = \frac{\dot{\phi}_c(0)}{\dot{\phi}(\tau)} \quad (6)$$

While assuming that the envelope  $A(t)$  of equation (1) is slowly varying, Carmona et al. [26] approximate the modulus of Morlet-Wavelet transform for any given signal with slow varying envelope as:

$$|W(s, \tau)| \approx \frac{1}{\sqrt{|s|}} A(\tau) |\Psi^*(s\dot{\phi}(\tau))| \quad (7)$$

Thus, from equation (6), the instantaneous frequency of the analytical solution can be obtained from the ridge extraction of Wavelet transform. Once the ridge and instantaneous frequencies are known, the envelope of the signal  $y(t)$  can be recovered following equation (7), and some modal parameters can be reconstructed following the same concept as in the Hilbert technique.

### 1.2 Detecting and Quantifying Chaos

Lin [20] shows theoretically that under certain excitations, a simple nonlinear mechanical system with backlash might manifest chaotic vibration. He demonstrates that a simple system comprising a backlash spring, as shown in Figure 1, and having a dynamic equation of:

$$m\ddot{x} + c\dot{x} + k_1 x + F(x) = A \cos \omega t$$

where  $F(x)$  is the restoring force of the nonlinear backlash component:

$$F(x) = \begin{cases} k_0(x - x_0 \cdot \text{sign}(x)) & , |x| \geq x_0 \\ 0 & , |x| < x_0 \end{cases}$$

is found to behave chaotically under certain excitation conditions. Table 1 gives three sets of system's parameters pertaining to chaotic behaviour, for certain excitation force specifications, where  $m$  is the mass of the system,  $k_1$  and  $k_0$  are stiffnesses,  $c$  is a damping coefficient, and  $x_0$  the backlash (or play) size.

It can be shown that there exist certain sinusoidal excitation forces for CASE 1, with  $A = |F| = 100$  N and for CASE 2 with  $A = 240$  N, both at  $\omega = 40$  rad/s, which cause the response to behave chaotically as the phase plots are shown in Figure 2. The bottom left figure shows the phase plot of CASE

3 under excitation of sinusoidal signal with  $A = 0.048$  N at 1.57 Hz, while the right panel represents the phase plot in the space of displacement with different time delay.

In order to examine the influence of each parameter on the nature of resulting response, we use dimensional analysis to normalise the variables and reduce the number of parameters. By combining variables in dimensionless groups, one may gain more insight in the problem.

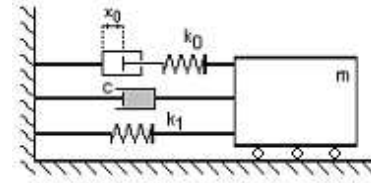


Figure 1. Schematic of a nonlinear mechanical system with backlash component.

Table 1. Parameter sets of vibration system

	$m$ (kg)	$k_1$ (N/m)	$k_0$ (N/m)	$c$ (Ns/m)	$x_0$ (m)
CASE 1	1	0	40000	8	0.005
CASE 2	1	1000	31000	8	0.005
CASE 2	3	0	2250	8	0.02

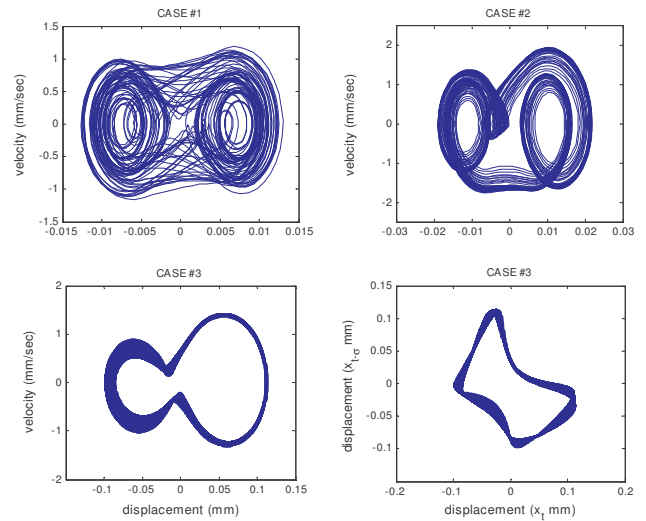


Figure 2. Phase plots of the chaotic response of two different mechanical systems with backlash component.

Introducing new variables of time and displacement  $\tau = \omega_0 t$  and  $p = x/x_0$ , where  $\omega_0^2 = k_0/m$ , we may rewrite the dynamics equation for CASE 1 ( $k_1 = 0$ ) as follows:

$$m\omega_0^2 x_0 p'' + c\omega_0 x_0 p' + k_0 x_0 \bar{F}(p) = A \cos \omega t \quad (8)$$

where the primes indicate differentiation with respect to  $\tau$  and  $\bar{F}$  is the backlash spring function. This equation reduces to:

$$p'' + 2\zeta p' + \bar{F}(p) = \alpha \cos \omega t \quad (9)$$

where  $2\zeta = c/\sqrt{k_0 m}$  and  $\alpha = A/(k_0 x_0)$  and  $\bar{F}(p)$  is backlash stiffness characteristic in normalized form:

$$\bar{F}(p) = \begin{cases} (p - \text{sign}(p)) & , |p| \geq 1 \\ 0 & , |p| < 1 \end{cases}$$

That is to say that the problem is characterized by two parameters,  $\alpha$  and  $\zeta$ .

As for the chaos measure, we calculate the maximum Lyapunov exponent of the resulting response. This is based on a unique property of chaotic behavior that two trajectories starting very close together will rapidly diverge from each other. The divergence (or convergence) of two neighboring trajectories can be used as a chaos quantification measure, which is the Lyapunov Exponent ( $\lambda$ ).

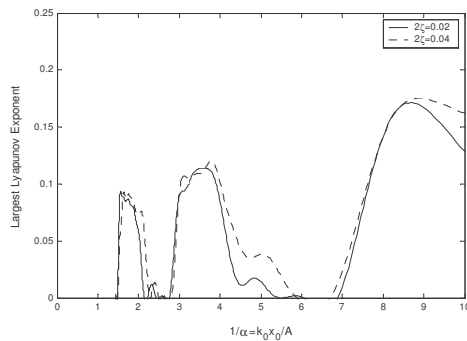


**Figure 3. The Largest Lyapunov Exponent vs  $1/\alpha$  for a simple mechanical system with backlash for CASE #1. The regions where the Lyapunov exponents are positive mark the presence of the chaotic response.**

Let us consider two initial conditions in a space  $x_0$  and  $x_0 + \delta_0$ , each of which will generate an orbit in the space using system equations. These orbits can be thought of as parametric functions of a variable (in general considered to be time). If we use one of the orbits as a reference orbit, then the separation between the two orbits will also be a function of time ( $\delta_t$ ).

In a system with attracting fixed points,  $\delta_t$  diminishes asymptotically with time. But for chaotic system, the separation between two trajectories will diverge exponentially fast; hence  $\delta_t$  will be an exponential function of time:

$$\delta_t = \delta_0 e^{\lambda t} \quad (10)$$

In order to see how a chaotic motion evolves when the forcing amplitude decreases (or equivalently the backlash size decreases), we generate the relationship between the largest Lyapunov Exponential and the parameter  $1/\alpha$  for CASE 1; and Figure 3 presents the results.

## 2 EXPERIMENTAL STUDY

An experimental investigation was carried out on the outer (second) link of a two-link mechanism as schematically shown in Figure 4.

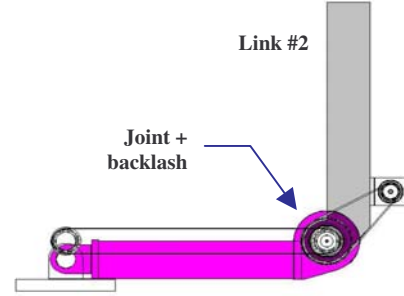


**Figure 4. Schematic drawing of a two-link mechanism.**

The aim of this experiment is to identify the backlash size of the second link joint. For this purpose, certain degree of backlash (approximately  $1.5^\circ$ ) was introduced in the joint of this link. The first link was kept fix while the second one was made to oscillate over a certain range. This link was driven by a servomotor through a toothed belt and a harmonic drive. The vibration responses were measured with two rotary encoders. First encoder measured the angular motion input to the harmonic drive, and the second one measured the relative oscillation between first link and second link. Therefore, the first encoder might be considered to measure excitation input of a *base motion system* in displacement form, while the second encoder measured the response of the base motion system.

### 2.1 Skeleton Identification

In the case of considering the experimental setup as a base motion system, where the excitation input is taken in the form of displacement, we need a little mathematical manipulation to reformulate equation (3).

Figure 5 depicts the schematic force balance of link#2 of the two-link system. The link is supported at its joint by a nonlinear rotational spring and damper. The support of this link has a specified rotational motion,  $\phi$ , which is the ‘displacement’ input, and is measured by first encoder. Angular motion of link #2 is represented by  $\theta$ .

The nonlinear differential equation of motion of the corresponding system can be obtained as follows:

$$J\ddot{\theta} + c(A)\dot{\theta} + \{k(A) - mgL\}\theta = c(A)\dot{\phi} + k(A)\phi \quad (11)$$

Following the notation of equation (1), i.e. replacing  $y$  by  $\theta$  and  $x$  by  $\phi$ , we get:

$$\ddot{y} + 2h_0(A)\dot{y} + \{\omega_0^2(A) - C\}y = 2h_0(A)\dot{x} + \omega_0^2(A)x$$

where  $C = mgL/J$  is an additional stiffness due to the link weight,  $m$  is mass of the link,  $L$  is the coordinate of the centre of gravity of the link and  $J$  equals the link’s moment of inertia about its joint.

Representing equation (11) into a displacement equation of a base motion system we obtain:

$$\ddot{z} + 2h_0(A)\dot{z} + \omega_0^2(A)z = -\ddot{x} + Cy, \quad (z = y - x) \quad (12)$$

If we refer to the transformation from displacement equation to complex-analytic signal form from reference [18], by analogy

we can transform equation (12) into complex-analytic signal form:

$$\ddot{Z} + 2h_0(A)\dot{Z} + \omega_0^2(A)Z = -\ddot{X} + CY \quad (13)$$

### 2.1.1 Signal Analysis

The experiments were taken by exerting linear chirp signal to the motor. Initial frequency of this signal is 0 Hz. The frequency continues to change at constant rate, and it reaches 12 Hz in 30 sec.

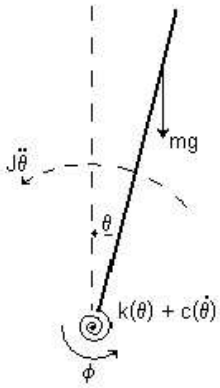


Figure 5. Force balance diagram of link #2

Relative motion measured by both encoders, where in equation (13) is represented by  $z$ , can be seen in Figure 6. It is seen from that figure, that the relative motion is higher than the backlash size in the joint. In the figure, the dash lines represent size of the backlash. At time 16.25 sec, which corresponds approximately to 6.5 Hz of excitation frequency, the relative motion of the link falls far below the size of backlash. This occurs due to insufficient energy of excitation. Such problem might cause unsatisfactory skeleton

curve reconstruction, which is essential in modal parameter identification.

In order to check the validity of these identification techniques, the system has been modally identified at the edge of backlash. Figure 7 shows the FRF of the system obtained through shock excitation using impact hammer. The link was preloaded using a low stiffness spring to eliminate nonlinearity due to the backlash; hence the link was resting on one of the edges of the backlash. It can be seen from the figure, that the natural frequency of the system is approximately 11 Hz, while from the mass line we can estimate the moment of inertia of the link to be approximately equal to 3.16 kgm<sup>2</sup>. It is necessary to define the inertia of the system, as far as equations (4a) and (4b) include modal mass value, which is unknown a priori.

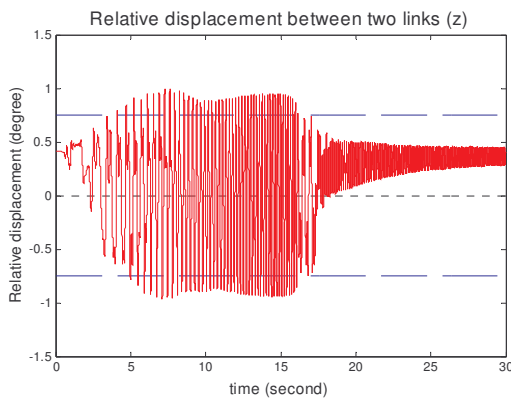


Figure 6. Relative motion between both links ( $z$ )

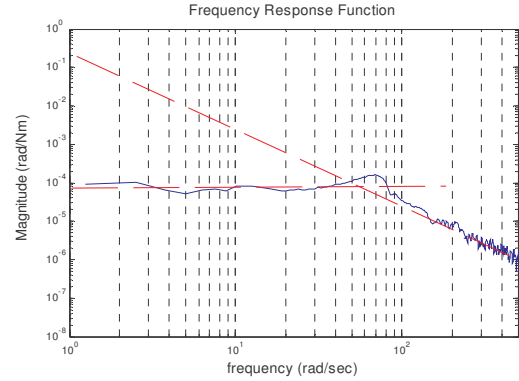


Figure 7. Frequency Response Function of two-link mechanism

### 2.1.2 Modification in nonlinear modal parameters calculation

Some obvious modifications of nonlinear modal parameter estimation procedures in equations (4) have to be made in order to conform to the base motion case, since we are dealing with displacement input and displacement output in the system [27].

The displacement input  $x(t)$ , in complex-analytic form appearing in equation (13), can be written as:

$$X(t) = x(t) + j\tilde{x}(t) = B(t) \cdot \exp[j\psi_x(t)]$$

The two derivatives of  $X(t)$  are then:

$$\dot{X}(t) = X(t) \left[ \dot{B}(t)/B(t) + j\dot{\omega}_x(t) \right]$$

$$\ddot{X}(t) = X(t) \left[ \ddot{B}(t)/B(t) - \omega_x^2(t) + 2j\dot{B}(t)\dot{\omega}_x(t)/B(t) + j\dot{\omega}_x(t) \right]$$

Substituting all of analytic signals and their derivatives in equation (13) we can get:

$$Z \left\{ \left( \frac{\ddot{A}}{A} - \omega^2 + \omega_0^2 + 2h_0 \frac{\dot{A}}{A} \right) + j \left( 2 \frac{\dot{A}}{A} \omega + \dot{\omega} + 2h_0 \omega \right) \right\} = -X \left\{ \left( \frac{\ddot{B}}{B} - \omega_x^2 \right) + j \left( 2 \frac{\dot{B}}{B} \omega_x + \dot{\omega}_x \right) \right\} + CY \quad (14)$$

Using the same procedures in equations (4) by solving two equations from the real and imaginary parts of equation (14), we can obtain the expression for instantaneous modal parameter as functions of first and second derivatives of signal envelopes and instantaneous frequencies of input and output displacement signal.

After identification, the restoring force, which illustrates the nonlinear spring characteristic of the system, and the damping force can be obtained based on the relations:

$$f_s(A) = A \cdot \omega_0^2(A) \quad (15)$$

$$f_d(\dot{A}) = 2h_0(A) \cdot \dot{A} \quad (16)$$

### 2.1.3 Identification Result

Envelope and instantaneous frequency calculation of both input ( $x$ ) and relative output signal ( $z$ ) can be seen in Figure 8 and Figure 9, respectively. In the left side of both figures, we can see the envelope estimation of displacement input and displacement output. The light-green dashed lines represent the envelope estimation based on Hilbert transform technique

without any filtration. The filtered HT curves represent the results of the envelope signal after low-pass filtration of 1% of its half sample rate (100% correspond to half the sample rate), while WT curves represent that of Wavelet Transform technique.

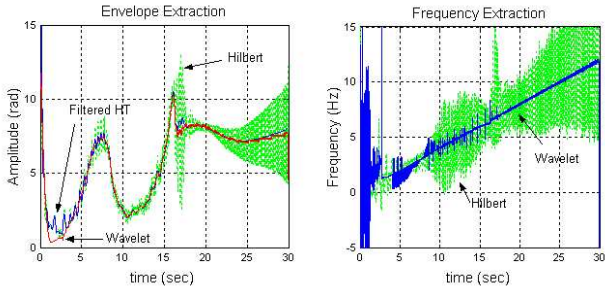


Figure 8. Envelope and instantaneous frequency of input signal

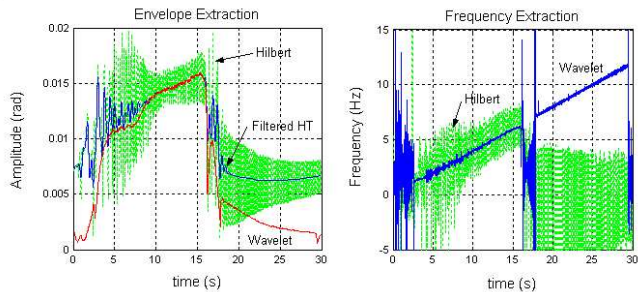


Figure 9. Envelope and instantaneous frequency of output signal

From these two figures, we can see that Wavelet analysis gives an improvement in estimation envelope and instantaneous frequency at several points. The most significant improvement is in the envelope and instantaneous frequency estimation of displacement output approximately after the first 17 seconds. If we refer back to Figure 6, it is clearly seen that the response is shifted after 17 seconds. This might have happened because at the corresponding time, the level of displacement input has fallen below the backlash size in the system. Hilbert Transform technique cannot estimate the envelope and also instantaneous frequency of a signal with certain offset. This is another advantage of Wavelet analysis.

At approximately time 16-17 seconds; we can see a significant estimation error in instantaneous frequency. In this instance, the estimation cannot be made in this region, since the frequency content of vibration response in this instance corresponds to the resonance frequency of the system.

Restoring Force and Damping Force

The restoring force as function of displacement can be derived utilising equations (4). The plot of this restoring force is shown in Figure 10. In the left side of Figure 10, we can see the restoring force estimation based on Hilbert transform technique with low-pass filtration of 1% of half of its sample rate, respectively. In the right side, we see the estimation based on Wavelet analysis. The size of backlash obtained from both techniques closed to the real backlash size introduced in the system. Based on the a priori knowledge of the system, by

applying regression on the reconstructed restoring force, we get the backlash size of 0.0258 rad (=1.48° with standard deviation of error below 1.5%), where the real backlash size is approximately 1.5° from manual measurement.

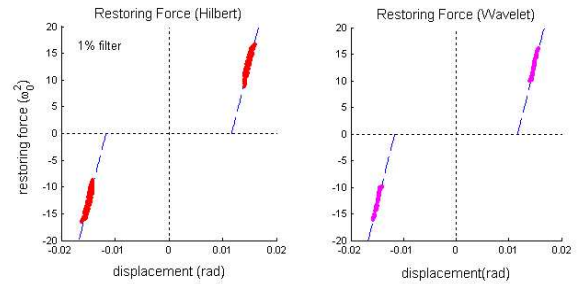


Figure 10. Restoring force estimation based on Hilbert and Wavelet transform

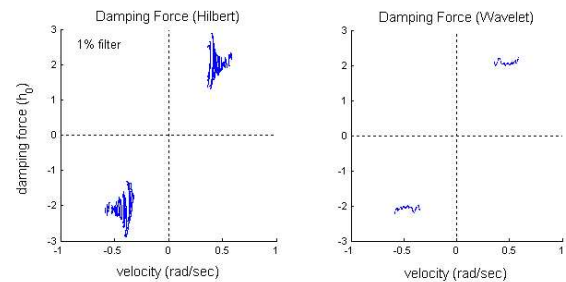


Figure 11. Damping force estimation based on Hilbert and Wavelet transform

Referring to equation (4a), the slope of the restoring force curve in Figure 10 actually represents the modal stiffness of the system. After multiplying the slope by moment of inertia of the second link, we can obtain the estimated stiffness value of the system. The modal stiffness parameter obtained by applying regression to the result is approximately 11000 Nm/rad.

The discontinuity appearing in the figures is due to the response at the resonance region as mentioned before. Hence, we cannot obtain the restoring force estimation in the corresponding region.

We can also identify the damping as a function of velocity by utilising equation (4b). Figure 11 shows the plot of the corresponding force, where the left figure shows the estimation based on the Hilbert analysis and the right one demonstrates the result based on the Wavelet analysis. The Hilbert based result shows imperfect reconstruction of the damping force and it suffers from more ripples than that of the restoring force. These are caused by the derivative form of the ‘noisy’ envelope function,  $\dot{A}$ , obtained from the Hilbert analysis, which is required in estimating the damping force as shown in equation (16).

Observing the behaviour, it is clearly seen that the damping force appears predominantly to be made up of friction, as a discontinuous constant force in zero velocity, as we can see in the plot, leads us to the signature of the friction force.

## 2.2 Chaotic response case

Under large amplitude excitation of a periodic force, it is found that the link system shows aperiodic behavior as can be observed from Figure 12. For this case, the system was excited by periodic motion with 1.54 Hz fundamental frequency and amplitude of  $2.68^\circ$ . However, we cannot ascertain whether this aperiodic response is dominated by the presence of linearly correlated noise.

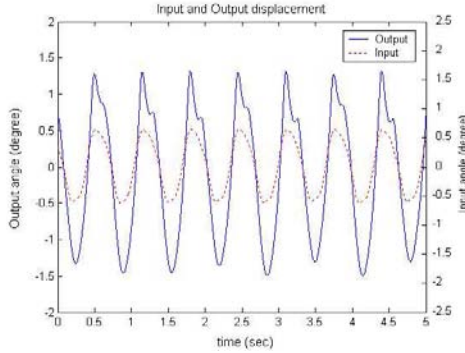


**Figure 12. Output response at 1.54 Hz and  $2.68^\circ$  input excitation. The solid line represents the output response while the dashed line is the input excitation. The left-scale is for the output and the right-scale is for the input.**

With the aim of having better understanding on how the chaotic motion arises when the modal parameters of the system change, in particular the backlash size (as implied by  $\alpha$  in dimensional analysis), the experiment was also carried out in several different excitation levels ranging from  $1.34^\circ$  to  $5.73^\circ$ , where it was observed that the aperiodic response persisted.

### 2.2.1 Quantifying chaos

The easiest way in obtaining the Lyapunov exponent, for instance, can be done by observing the separation of two close initial trajectories on the attractor and taking the logarithm of the separation. But this method cannot be applied directly to experimental data for the reason that we are not always dealing with two (or more) sets of experimental data that have close initial conditions.

Experimental data typically consists of single observable discrete measurements. Reconstructing the phase space from the time series with appropriate time delay and embedding dimension makes it possible to obtain an attractor whose Lyapunov spectrum is identical to that of the original attractor. Mathematically, a reconstructed phase space can be described as follows [28,29]:

$$y(k)=[S(k), S(k+\tau), S(k+2\tau), \dots, S(k+(d-1)\tau)] \quad (17)$$

where  $S(k)$  is the time series from a single observation,  $\tau$  represents appropriate time delay for phase space reconstruction and  $d$  is a proper embedding dimension for phase space reconstruction.

Now, if we choose two points in the reconstructed phase space whose temporal separation in the original time series is at least one 'orbital period', they may be considered as different trajectories on the attractor. Hence, the next step in determining

the largest Lyapunov exponent for single observable time series is searching the nearest neighbor of certain points, in the sense of Euclidean distance, which can be considered as fiducial trajectories.

In a phase space reconstruction procedure, we must ensure that the points in each dimension (coordinate) are independent of each other. Therefore, time delay  $\tau$  must be chosen so as to result in points that are not correlated to previously generated points. The *Average Mutual Information* (AMI) technique can be used for determining appropriate time delay parameter for nonlinear time series. Abarbanel [30] suggested that the value of  $\tau$  for which the first local minimum of the AMI occurs should be taken as time delay, and this is analogous to the time delay when the auto-correlation function attains zero value in linear case. Figure 13 shows the mutual information of the response shown in Figure 12. The first minimum value of the mutual information is approximately 0.174 sec.

The next step in reconstructing phase space is to recover the appropriate number of coordinates  $d$  of the phase space. The idea of a number of coordinates  $d$  is a dimension in which the geometrical structure of the phase space is completely unfolded.

The basic method in determining the embedding dimension in phase-space reconstruction is the *False Nearest Neighbor* method. Suppose the vector  $y^{NN}(k)$  is a false neighbor of  $y(k)$ , having arrived in its neighborhood by projection from a higher dimension, because the present dimension  $d$  does not unfold the attractor, then by going to the next dimension  $d+1$ , we may move this false neighbor out of the neighborhood of  $y(k)$ . Thus, if the additional distance is large compared to the distance in dimension  $d$  between nearest neighbors, we have a false neighbor. Otherwise, we have a true neighbor.

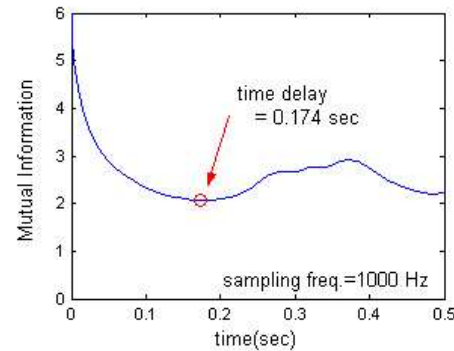


**Figure 13. Average mutual information as a function of the time lag for CASE 1 system excited by  $2.68^\circ$  input excitation.**

In order to have a straightforward representation of the minimum embedding dimension, Cao [31] defined the mean value of  $E1$ , which generally represents the relative Euclidean distance between  $y^{NN}(k)$  and  $y^{NN}(k)$  in two consecutive dimensions. Cao's number  $E1$  consequently will stop changing when the dimension  $d$  is greater than the minimum embedding dimension  $d_0$ .

Figure 14 depicts the Cao number as a function of embedding dimension. It can be observed that E1 approaches a constant value for a dimension higher than four. Thus, we can conclude that the minimum dimension that will totally unfold the phase space is 5.

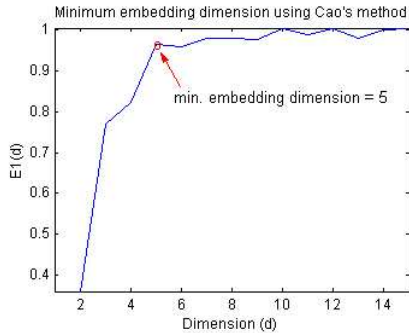


**Figure 14. Minimum embedding dimension for CASE 1 system excited by 2.68° input excitation.**

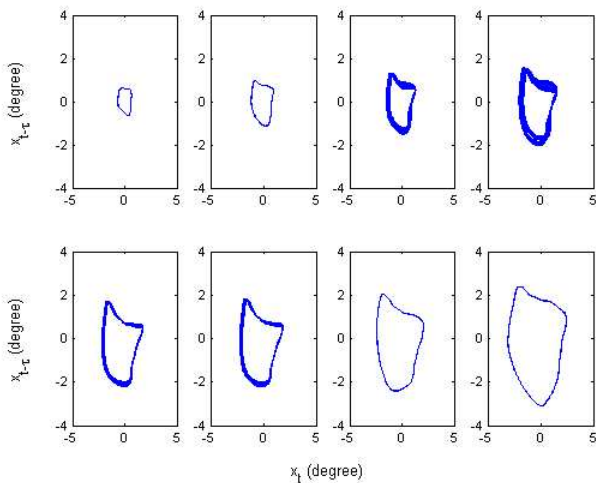


**Figure 15. Phase plots of output responses with certain discrete unit time delay of corresponding mechanical system with excitation frequency of 1.54 Hz and amplitude level respectively from left to right and top to bottom: 1.34°; 2.07°; 2.68°; 3.41°; 3.65°; 3.78°; 4.87°; 5.73°.**

Repeating the above sequences for different excitation levels ranging from 1.34° to 5.73° as mentioned before, we obtain the phase-space plots as shown in Figure 15. The figure shows the phase plots of output responses with certain time delays, which are determined using the *Average Mutual Information* method. Observing the figures, we may suspected that the excitation level of 2.68°, 3.41°, 3.65° and 3.78° result in chaotic responses.

### 2.2.2 Surrogate data testing

Nevertheless, from the results we have so far, it is not clear in any of the cases if noise (linearly stochastic process) is not the cause for the observed irregular behavior. Surrogate data test is utilized to identify whether the behavior of a signal is caused by the nonlinearity in the system or by a random

stochastic process. This method first specifies some linear process as a null hypothesis, then generates surrogate data sets, which are consistent with this null hypothesis, and finally computes a discriminating statistics for the original and for each of the surrogate data sets. In order to generate the surrogate data sets, the original data are transformed in such a way that all structures except for the assumed properties are destroyed. The generated surrogate data sets are assumed to mimic only the linear properties of the original data. Theiler et al. [32] state that a Fourier Transform algorithm is very consistent with the hypothesis of linearly correlated noise. This method is achieved by Fourier transforming the original data and substituting the phases with random numbers. After transforming back into the time domain, we get a new time series without affecting the power spectrum. If the discriminating statistic values (namely the maximum Lyapunov exponent, the average mutual information and/or the correlation dimension) computed for the original data is significantly different from the generated surrogate data, then the null hypothesis is rejected and we conclude that the data is not linearly stochastic noise and the nonlinearity is detected.

Since we are motivated by the possibility that the underlying dynamics may be chaotic, our original choices for discriminating statistics are the chaotic quantifications. The correlation dimension,  $D_2$ , is the most frequently used as a discriminating statistic in surrogate data test.  $D_2$  is computed as a limit of the correlation sum or the correlation integral [30]:

$$D_2 = \lim_{r \rightarrow 0} \frac{\log |C(2, r)|}{2 \log |r|}$$

where  $C(2, r)$  counts all the points within distance  $r$  of each other.

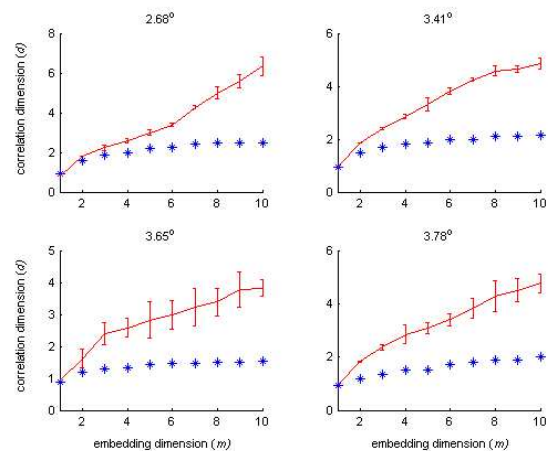


**Figure 16. The correlation dimension versus embedding dimension for the original data (excited at excitation level 2.68°, 3.41°, 3.65° and 3.78°) and for the surrogates. The values of the correlation dimension for the original data and the surrogates differ substantially, and the convergence value of the original data suggests that the underlying dynamics is chaotic.**

Generally, if the irregularity in the data is chaotic, going to a higher embedding dimension will not change the result of  $D_2$ .

On the contrary, if the data is in fact noise, the correlation dimension will not converge to a specific value in going to a higher embedding dimension.

Figure 16 shows the plots of the correlation dimension as the discriminating statistics against the embedding dimension,  $m$ , for four suspected chaotic responses in Figure 15 (excited at levels  $2.68^\circ$ ,  $3.41^\circ$ ,  $3.65^\circ$  and  $3.78^\circ$ ). All of the plots in Figure 16 show that for all the cases, the values of the correlation dimension for the original data and the surrogates differ substantially. We can also conclude that the figures show the convergences of the correlation dimension for the original data, while the surrogates show no convergences. The estimated dimensions of the original data about  $d = 2.50$ ,  $2.10$ ,  $1.55$  and  $2.10$  in ascending excitation level order, respectively, shows that the underlying dynamics is in fact chaotic.

### 2.2.3 Noise reduction

A story of an experimental analysis is never complete without discussing the noise reduction step. The noise reduction step plays an important role in estimating the largest Lyapunov exponent to quantify chaotic behaviour. One of the problems in estimating the largest Lyapunov exponent of a 'noisy' signal concerns the minimum embedding dimension required to completely unfold the noisy attractor of the signal. The *Simple Noise Reduction* [33] will be utilized in this work, since it offers superiority, in the calculation time, and simplicity.

The Simple Noise Reduction techniques are closely related to the future prediction theory. For prediction we have no information about the quantity to be forecast other than the preceding measurement, while for noise reduction we have a noisy measurement to start with and we have the future values. Hence we aim to replace the noisy measurement with a set of 'predicted values' containing errors, which are on average less than the initial amplitude of the noise.

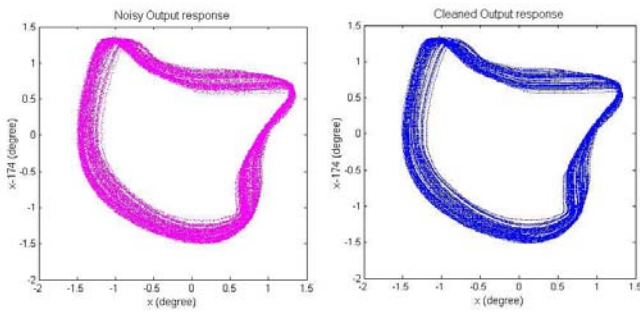


Figure 17. Cleaned signal compared to the noisy one. The left figure shows the phase plot of the response of the system under excitation frequency of 1.54 Hz and amplitude level of  $2.68^\circ$  before noise reduction, while the cleaned signal can be seen in the right figure.

Figure 17 shows the result of simple noise reduction method of output response when the system was excited using  $3.41^\circ$  excitation level, compared to the un-cleaned one. One

may see that the trajectory appears smoother after noise reduction. Verification and quantification of the noise reduction performance can be done on the basis of the correlation integral. For our case, since the noise level is not significantly high, this verification will not be discussed in this paper.

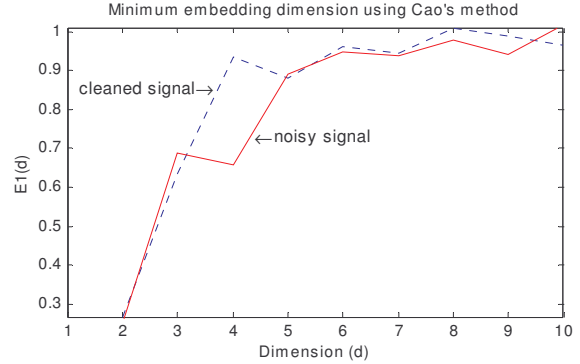


Figure 18. Estimation of minimum embedding dimension of noisy and cleaned signals using Cao's method. The noisy signal needs more dimensions to completely unfold the attractor compared to the cleaned one.

In Figure 18, we can see the plot of the Cao's number  $E1$  versus its embedding dimension  $d$ . The solid line represents  $E1$  for original noisy signal, while the dashed line represents  $E1$  for the signal when its noise has been reduced. From the figure, we can see that the noisy signal needs a higher dimension to unfold its attractor compared to its cleaned counterpart. The noisy one takes a minimum of 5 embedding dimensions to completely unfold its attractor, while the cleaned one needs only 4.

### 2.2.4 Maximum Lyapunov exponents

Having reconstructed phase spaces of the cleaned signals, the final step is determining the Lyapunov exponents of the corresponding signals. Table 2 shows the chaos quantification of Lyapunov exponents for corresponding results in Figure 15, starting from the lowest excitation level to the highest respectively. The evolution of the Lyapunov exponents as shown in the table obviously marks the bifurcation phenomenon in the system. The response behaves periodically at low excitation levels until it reaches certain level between  $2.07^\circ$  and  $2.68^\circ$ , then the chaotic response grows. Subsequently, after certain excitation level (between  $3.78^\circ$  and  $4.87^\circ$ ), the chaotic behavior diminishes, and the response, again, behaves periodically.

Table 2. Chaotic quantification results of series excitation

Exc. Level	$1.34^\circ$	$2.07^\circ$	$2.68^\circ$	$3.41^\circ$
$\lambda$ (bit/time)	-	-	1.423	1.322
Exc. Level	$3.65^\circ$	$3.78^\circ$	$4.87^\circ$	$5.73^\circ$
$\lambda$ (bit/time)	1.533	1.802	-	-

### 3 CONCLUSION

Nonlinear modal parameters estimation technique based on Hilbert and Wavelet transform are shown to be a good approximation of the true modal parameters characteristic. Both the backlash size and the stiffness can be estimated satisfactorily.

An improvement of nonlinear modal parameters estimation by introducing Wavelet analysis has been achieved owing to several advantages offered by Wavelet properties. Wavelet transform is capable of analysing envelope and instantaneous frequency of a shifted signal and the results have less-wiggles compared to those of Hilbert transform. However, there are some drawbacks in the Wavelet based technique. It needs not only a large amount of computation memory for its calculation process, since it deals with time-frequency domain, but also a long processing time.

A major difficulty in utilising the methods introduced in this paper concern the level of displacement input applied to the system. This displacement input should have an adequate level to ensure covering the backlash size. Due to the limitation of energy of excitation, this might become a problem, especially at high frequency. Limited level of displacement input will yield only a partial reconstruction of the restoring force characteristics.

Finally, under certain excitation conditions, there may exist some separate regions for which chaotic vibrations could occur. The transition to and from those regions is marked by bifurcation points. We have shown that, for this case, it would be possible to quantify the Lyapunov exponent, for each amplitude of excitation. Correlating the Lyapunov exponent with  $\alpha = A/k_0x_0$  could, in principle, yield the backlash size. Hence, although quite difficult to perform in practice, chaos quantification could be used as a quantitative mechanical signature of a backlash component.

### ACKNOWLEDGMENTS

The authors wish to acknowledge the partial financial support for this study by the Volkswagenstiftung under grant No. I/76938.

### REFERENCES

1. K. Wyckaert, Development and Evaluation of Detection and Evaluation Schemes for the Nonlinear Dynamical Behaviour of Mechanical Structures, PhD Thesis, Department of Mechanical Engineering, Division PMA, Katholieke Universiteit Leuven, 1992.
2. G. Tomlinson, *Detection, Identification and Quantification of Nonlinearity in Modal Analysis*, Proceeding of the Fifth International Modal Analysis Conference, London, 1987.
3. K. Worden, G.R. Tomlinson, *Nonlinearity in Structural Dynamics*, Institute of Physics Publishing, Bristol and Philadelphia, USA, 2001.
4. <http://zone.ni.com/devzone/nidzgloss.nsf/webmain/2579395D1F8016700625687F0061BDF1>
5. G. R. Tomlinson, *Developments in The Use of The Hilbert Transform for Detecting and Quantifying Non-Linearity Associated with Frequency Response Functions*, Mechanical Systems and Signal Processing 1(2) (1987) 151-171.
6. M. Feldman, *Non-Linear System Vibration Analysis Using Hilbert Transform-I. Free Vibration Analysis Method 'FreeVib'*, Mechanical Systems and Signal Processing 8(2) (1994) 119-127.
7. M. Feldman, S. Braun, *Analysis of Typical Nonlinear Vibration Systems by Using the Hilbert Transform*, Proceedings of the XI Int. Modal Analysis Conference, Kissimmee, Florida, 1993, pp. 799-805.
8. S. Braun, M. Feldman, *Time-Frequency Characteristics of Non-Linear Systems*, Mechanical Systems and Signal Processing, 11(4) (1997) 611-620.
9. M. Feldman, *Non-Linear Free Vibration Identification Via The Hilbert Transform*, Journal of Sound and Vibration, 208(3) (1997) 475-489.
10. P. Davies, J.K. Hammond, *The use of envelope and instantaneous phase methods for the response of oscillatory nonlinear systems to transients*. Proceedings of the 5<sup>th</sup> IMAC, Vol. II, 1987, pp.1460-1466.
11. M. Feldman, S. Seibold, *Damage Diagnosis of Rotors: Application of Hilbert Transform and Multi-Hypothesis Testing*, Journal of Vibration and Control, 5 (1999) 421-445.
12. L. Wang, J. Zhang, C. Wang, S. Hu, *Time-Frequency Analysis of Nonlinear Systems: The Skeleton Linear Model and the Skeleton Curves*, Transaction of the ASME, 125 (2003) 170-177.
13. M. Feldman, *Non-Linear System Vibration Analysis Using Hilbert Transform-II. Forced Vibration Analysis Method 'ForceVib'*, Mechanical Systems and Signal Processing 8(3) (1994) 309-318.
14. M. Ruzzene, L. Fasana, L. Garibaldi, B. Piombo, *Natural Frequencies and Dampings Identification Using Wavelet Transform: Application to Real Data*, Mechanical Systems and Signal Processing (1997) 11(2), pp. 207-218.
15. M. Feldman, S. Braun, *Identification of Nonlinear System Parameters via the Instantaneous Frequency: Application of the Hilbert Transform and Wigner-Ville Techniques*, Proceeding of the XIII International Modal Analysis Conference, Nashville, Tennessee, 1995, pp. 637-642.
16. R. Ghanem, F. Romeo, *A Wavelet-Based Approach for The Identification of Linear Time-Varying Dynamical Systems*, Journal of Sound and Vibration, 234(4) (2000) 555-576.
17. V. Lenaerts, G. Kerschen, J.C. Golinval, M. Ruzzene, F. Giorcelli, *Validation of Two Nonlinear System*

- Identification Techniques Using an Experimental Testbed*, Shock and Vibration, 11 (2004) 365-375.
18. W.J. Staszewski, *Identification of Nonlinear Systems Using Multy-Scale Ridges and Skeletons of The Wavelet Transform*, Journal of Sound and Vibration (1998) 214(4), pp. 639-658.
  19. W.J. Staszewski, J.E. Chance, *Identification of Nonlinear Systems Using Wavelets – Experimental Study*, Proceedings of the XV International Modal Analysis Conference, Orlando, FL, 1997, pp. 1012-1016.
  20. R.M. Lin, *Identification of The Dynamic Characteristics of Nonlinear Structures*, PhD Thesis, Mechanical Engineering Department, Imperial College of Science, Technology and Medicine, London, UK, 1990.
  21. S. Theodossiades, S. Natsiavas, *Nonlinear Dynamics of Gear Pair Systems with Periodic Stiffness and Backlash*, Journal of Sound and Vibration 229(2) (2000) 287-310.
  22. Q. Feng, and F. Pfeiffer, *Stochastic Model on A Rattling System*, Feng, Q., and Pfeiffer, F., Stochastic Model on A Rattling System, Journal of Sound and Vibration 104(2) (1998) 328-342.
  23. I. Trendafilova and H. Van Brussel, *Nonlinear Dynamics Tools for The Motion Analysis and Condition Monitoring of Robot Joints*, Mechanical Systems and Signal Processing, 15 (2001) 1141-1164.
  24. M. Misiti, Y. Misiti, G. Oppenheim, J.M. Poggi,, *Wavelet Toolbox for Use with Matlab*, The MathWorks, July 2002 (online only)
  25. P.H. Tchamitchian, B. Torr sani, *Ridge and Skeleton Extraction from the Wavelet Transform In Wavelets and Their Application*, in M.B. Ruskai, editor, Jones and Bartlett Publishers, 1992
  26. R.A. Carmona, W.L. Hwang, B. Torr sani, *Characterization of Signals by the Ridges of Their Wavelet Transforms*, IEEE Transactions on Signal Processing (1997) 45(10), pp. 2586-2590
  27. T. Tjahjowidodo, F. Al-Bender, H. Van Brussel, *Experimental Dynamic Identification of Backlash Using Skeleton Methods*, submitted to Mechanical Systems and Signal Processing, May 2005.
  28. A.A. Tsonis, *Chaos: From Theory to Applications*, Plenum Press, New York, 1992.
  29. R.C. Hilborn, *Chaos and Nonlinear Dynamics: An Introduction for Scientist and Engineers*, Oxford University Press, 1994.
  30. H. Abarbanel, *Analysis of Observed Chaotic Data*, Berlin: Springer-Verlag, 1996.
  31. L. Cao, A. Mees, K. Judd and G. Froyland, *Determining the Minimum Embedding Dimensions of Input-Output Time Series Data*, *International Journal of Bifurcation and Chaos*, 8 (1997) 1491-1504.
  32. J. Theiler, S. Eubank, A. Longtin, B. Galdrikian, J. Farmer, *Testing for Nonlinearity in Time Series: The Method of Surrogate Data*, *Physica* 58D (1992) 77-94.
  33. H. Kantz, T. Schreiber, *Nonlinear Time Series Analysis*, Cambridge University Press, 1997.
  34. T. Tjahjowidodo, F. Al-Bender, H. Van Brussel, *Quantifying Chaotic Responses of Mechanical Systems with Backlash Component*, submitted to Nonlinear Analysis: Real World Application, May 2005.